Acta Crystallographica Section D
Biological Crystallography
ISSN 0907-4449

Structure of an aryl esterase from *Pseudomonas fluorescens*

Jeremy D. Cheeseman,[a] Ante Tocilj,[b] Seongsoon Park,[a]‡ Joseph D. Schrag[b]* and Romas J. Kazlauskas[a]*§

[a]Department of Chemistry, McGill University, 801 Sherbrooke Street West, Montreál, Québec H3A 2K6, Canada, and [b]Biotechnological Research Institute, National Research Council of Canada, 6100 Royalmount Avenue, Montréal, Québec H4P 2R2, Canada

‡ Current address: Department of Biotechnology, Division of Biochemistry, Royal Institute of Technology (KTH), AlbaNova University Center SE-106 91, Stockholm, Sweden.
§ Current address: University of Minnesota, Department of Biochemistry, Molecular Biology and Biophysics and The Biotechnology Institute, 1479 Gortner Avenue, Saint Paul, Minnesota 55108, USA.

Correspondence e-mail: joe@bri.nrc.ca, rjk@umn.edu

Received 3 April 2004
Accepted 29 April 2004

PDB Reference: aryl esterase, 1va4, r1va4sf.

The structure of PFE, an aryl esterase from *Pseudomonas fluorescens*, has been solved to a resolution of 1.8 Å by X-ray diffraction and shows a characteristic α/β-hydrolase fold. In addition to catalyzing the hydrolysis of esters *in vitro*, PFE also shows low bromoperoxidase activity. PFE shows highest structural similarity, including the active-site environment, to a family of non-heme bacterial haloperoxidases, with an r.m.s. deviation in 271 C^{α} atoms between PFE and its five closest structural neighbors averaging 0.8 Å. PFE has far less similarity (r.m.s. deviation in 218 C^{α} atoms of 5.0 Å) to *P. fluorescens* carboxyl esterase. PFE favors activated esters with small acyl groups, such as phenyl acetate. The X-ray structure of PFE reveals a significantly occluded active site. In addition, several residues, including Trp28 and Met95, limit the size of the acyl-binding pocket, explaining its preference for small acyl groups.

1. Introduction

Pseudomonas fluorescens aryl esterase (PFE; EC 3.1.1.2) is one of several esterases in *P. fluorescens* (Choi *et al.*, 1990). Initial substrate mapping of PFE showed that it favors esters containing aryl alcohol moieties, such as phenyl acetate, and classsified PFE as an aryl esterase. Liu *et al.* (2001) extended the substrate mapping and confirmed the preference of PFE for aryl esters, but found that its preferred substrates are a wider range of activated esters. In addition to aryl esters, vinyl esters are good substrates, as are esters that contain an activating group in the acyl portion of the ester, *e.g.* α-halo activated esters. Choi and coworkers' initial substrate mapping also revealed a preference for esters with small acyl groups such as acetate. Propanoate and butanoate esters react more slowly, while benzoates and esters of longer-chain fatty acids do not react. Liu *et al.* (2001) confirmed this preference for small acyl groups, but found that esters with large acyl groups react slowly if they are activated esters, *e.g.* vinyl benzoate or vinyl trimethylacetate. Thus, PFE favors activated esters with small acyl groups. Other carboxylases from *P. fluorescens* have complementary substrate specificity: they prefer esters of longer-chain (C_2–C_6) fatty acids and do not accept esters with aryl alcohol moieties or even alcohol moieties larger than a methyl group.

PFE shows moderate to high enantioselectivity towards useful building blocks for organic synthesis. PFE shows high enantioselectivity in the acylation of racemic 1-phenylethanol with vinyl acetate in toluene and in the hydrolysis of the corresponding racemic acetate in water (Krebsfänger *et al.*, 1998). PFE also shows moderate enantioselectivity in the hydrolysis of methyl (*S*)-3-bromo-2-methylpropionate (MBMP) and methyl (*R*)-2-chloropropionate (Liu *et al.*, 2001).

Protein engineering can increase the enantioselectivity and reaction rate. A Thr229Ile mutation increases the enantioselectivity toward MBMP from 12 (wild type) to 19 (Horsman *et al.*, 2003). Homology modeling suggests that this mutation is ~13 Å from the active site. Mutagenesis of two residues closer to the active site, Trp28 and Val121, dramatically increases the enantioselectivity of PFE toward MBMP (Park *et al.*, 2004). A Leu180Gln mutation increases the reaction rate of PFE and increases its enantioselectivity towards (*R*)-3-phenylbutyric acid resorufin ester from 3.5 to 6.6 (Henke & Bornscheuer, 1999). A double mutation increased the reaction rate of PFE with a sterically hindered 3-hydroxy ester useful in the synthesis of epothilone A and B (Bornscheuer *et al.*, 1999).

PFE is closely related to a family of bacterial non-heme haloperoxidases. PFE has ~50% amino-acid sequence identity to these haloperoxidases and also shows low haloperoxidase activity: approximately 470 times lower than that of haloperoxidase from *P. pyrrocinia* (Pelletier & Altenbuchner, 1995). Conversely, this haloperoxidase showed low esterase activity: approximately 50-fold lower than that of PFE toward *p*-nitrophenyl acetate. The overlapping catalytic activity of these enzymes stems from common transition states and acyl-enzyme intermediates in both reactions (Fig. 1). In esterases, the acyl-enzyme intermediate reacts with water to give hydrolysis. In haloperoxidases, the acyl enzyme forms from acetate required in the solution and reacts with hydrogen peroxide to yield peroxyacetic acid. The subsequent oxidation of halide to hypohalous acid by peroxyacetic acid may not be enzyme-catalyzed, but reports of regioselective oxidations suggest that the enzyme is involved in some cases (Laatsch *et al.*, 1994; Picard *et al.*, 1997). Many lipases also catalyze a similar formation of peroxycarboxylic acids consistent with the common intermediates in ester hydrolysis and non-heme haloperoxidase activity (Björkling *et al.*, 1992; Kirk & Conrad, 1999). In spite of the overlapping activity, esterases show higher esterase activity, while haloperoxidases show higher haloperoxidase activity. A detailed analysis of the X-ray crystal structure of a chloroperoxidase (PDB code 1a8s; Hofmann *et al.*, 1998) did not identify any major features that would enhance chloroperoxidase activity or limit esterase activity.

This paper describes the first crystallization and structure determination of PFE and provides a structural basis for further application in biocatalysis. The structure qualitatively explains its substrate preferences for esters with small acyl groups and identifies residues close to the active site that may influence enantioselectivity. The closest structural neighbor of PFE is chloroperoxidase 1a8s, suggesting that PFE may be an evolutionary link between esterases and non-heme haloperoxidases. However, this comparison shows few differences and no obvious structural explanation for differences in catalytic specificity.

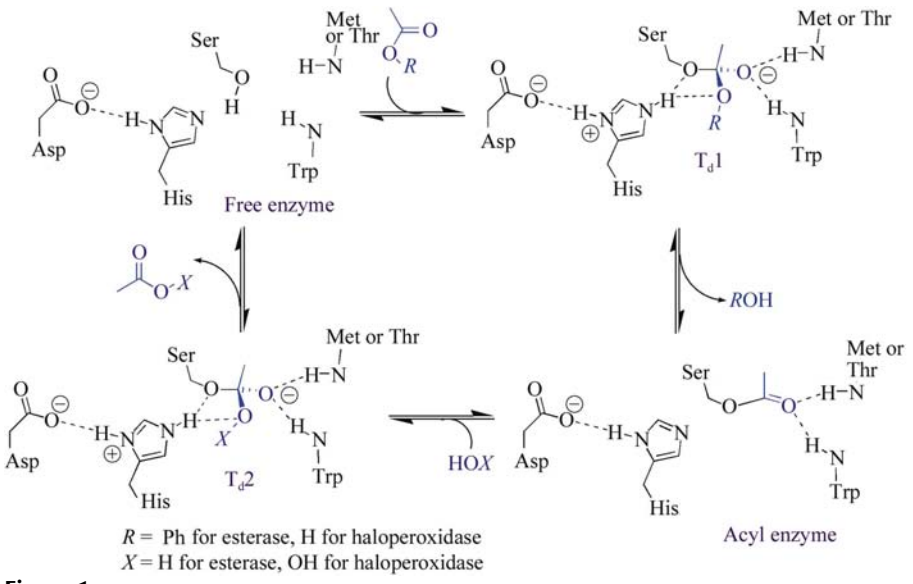

Figure 1
Ester-hydrolysis mechanism (left) and the postulated haloperoxidase mechanism (right) (Hofmann *et al.*, 1998). Both form an acyl-enzyme intermediate. In esterases, H_2O attacks this intermediate to complete hydrolysis. In haloperoxidases, the acyl-enzyme intermediate comes from acetate added to the reaction mixture. Hydrogen peroxide attacks this intermediate to form a peracid. The subsequent reaction of peracid with halide form hypohalous acid; the subsequent alkyl halogenation may not be enzyme-catalyzed.

2. Methods and materials

2.1. Expression and purification

A 1 ml overnight culture of recombinant *Escherichia coli* DH5α containing plasmid pJOE2792, which codes for PFE including a C-terminal His_6 tag, was added to Luria–Bertani broth (100 ml) and grown at 310 K, 200 rev min^{-1} to an OD_{600} of 0.5 (similar to Krebsfänger *et al.*, 1998). PFE expression was induced by adding sterile rhamnose [1 ml; 20%(*w*/*v*)] and the culture was incubated for 6 h at 310 K at 200 rev min^{-1}. The cells were harvested by centrifugation (15 min, 1900*g*, 277 K) and the supernatant was discarded. The cell pellet was resuspended in 4 ml buffer *A* (50 m*M* NaH_2PO_4, 300 m*M* NaCl, 10 m*M* imidazole adjusted to pH 8.0 with NaOH), to which lysozyme was added (1 mg ml^{-1}; 47 000 U mg^{-1}). After incubation at 310 K, 200 rev min^{-1} for 45 min, the cells were frozen to 253 K and then thawed. The viscosity of the lysate was reduced by repeatedly passing the solution through a 20-gauge needle to shear DNA/RNA. After centrifugation at 1900*g* for 45 min at 277 K, the supernatant (4 ml) was collected. Ni–NTA agarose slurry (2 ml, as a 50% slurry in 30% ethanol; Qiagen Inc, Mississauga, ON, Canada) was added to the remaining cleared lysate and the mixture was stirred at 277 K for 1 h. The mixture was loaded onto a Poly Prep column (BioRad, Hercules, CA, USA), allowed to settle and then drained. The Poly Prep

column now containing Ni–NTA with bound PFE was then washed twice with 4 ml buffer *B* (50 m*M* NaH_2PO_4, 300 m*M* NaCl, 20 m*M* imidazole adjusted to pH 8.0 with NaOH) to remove any non-specifically bound contaminants. The PFE enzyme was eluted from the column with 15 ml buffer *C* (50 m*M* NaH_2PO_4, 300 m*M* NaCl, 250 m*M* imidazole adjusted to pH 8.0 with NaOH). Eluate from the Ni–NTA column containing purified PFE was buffer-exchanged from buffer *C* to 5 m*M* BES pH 7.2 using a Macrosep centrifugal concentrator with 10 kDa molecular-weight cutoff (Pall Filtration Co., Northborough, MA, USA). After concentration and three washes, each with 10 ml of 5 m*M* BES buffer in the centrifugal concentrator (1900*g*, 90 min), the enzyme solution was concentrated to 15 mg ml^{-1} and used directly in crystallization trials.

2.2. Crystallization and data collection

Initial crystallization conditions for His-tag-purified PFE were identified by sparse-matrix screening using Hampton Crystal Screens I and II (Hampton Research, Laguna Niguel, CA, USA). Crystallization optimizations using precipitant solutions containing between 1 and 2 *M* $(NH_4)_2SO_4$ were performed using the hanging-drop vapor-diffusion method in a 24-well plate. The best crystals formed when protein drops were suspended above 1 ml of a precipitant solution consisting of 1.65 *M* $(NH_4)_2SO_4$, 1% PEG 400 in 0.1 *M* HEPES pH 7.5. Drops contained 3 µl of protein solution (15 mg ml^{-1}) and 5 µl precipitant solution. Crystals were flash-frozen at 93 K after brief immersion in a cryoprotectant solution consisting of precipitant solution with 25% glycerol added. Data were collected using a Rigaku Micromax 007 rotating-anode generator equipped with Osmic mirrors and an HTC image-plate detector (Rigaku/MSC; The Woodlands, TX, USA). Data were reduced using *d*TREK* (Pflugrath, 1999).

2.3. Structure solution and refinement

Phases were determined by molecular replacement using *MOLREP* (Vagin & Teplyakov, 1997) with chloroperoxidase 1a8s as a search model. Initial refinement was performed using *CNS* (Brünger *et al.*, 1998) and final refinements were performed using *REFMAC* (Murshudov *et al.*, 1997). No σ-cutoffs or non-crystallographic symmetry restraints were used in the refinements.

3. Results

3.1. Crystallization summary and statistics

Optimization around initial hits from the Hampton Research Crystal Screen conditions containing high concentrations (1.65 *M*) of ammonium sulfate yielded X-ray quality crystals of PFE. The largest crystals, measuring 1.4 × 0.8 × 0.3 mm, grew in one week and were hexagonal. In some cases, crystals grew as stacks of plates from which single crystals could be separated. Initial data were consistent with either space group $P3_1$ or $P3_2$, but the translation solution showed that $P3_2$ was correct. The asymmetric unit contained six molecules and had a solvent content of 72%. All data were collected from one crystal (Table 1).

Table 1
Data-collection and refinement statistics for *P. fluorescens* aryl esterase.

Data collection	
Space group	$P3_2$
Unit-cell parameters	
$a = b$ (Å)	146.0
c (Å)	129.9
$\alpha = \beta$ (°)	90.0
γ (°)	120.0
No. reflections	
Observed	1368717
Unique	271452
R_{sym} (%)	
Overall	6.6
Highest shell (1.87–1.80 Å)	24.7
Completeness (%)	
Overall	95.2
2.03–1.94 Å shell	97.1
Highest shell (1.85–1.80 Å)	65.8
$I/\sigma(I)$	
Overall	14.0
Highest shell (1.85–1.80 Å)	3.7
Refinement	
Resolution range (Å)	48.8–1.8
R_{work} (highest shell) (%)	17.5 (31.9)
R_{free} (highest shell) (%)	20.2 (34.4)
R.m.s. deviations from ideality	
Bond lengths (Å)	0.021
Bond angles (°)	1.51
Dihedral angles (°)	24.5
Improper angles (°)	1.72
Ramachandran analysis	
Most favored (%)	91.2
Allowed (%)	7.90
Generously allowed (%)	0.90
Disallowed (%)	0.00
Final model	
No. of atoms	
Protein	12720
Solvent (H_2O and glycerol)	1482
Mean B factor (Å^2)	
Main chain	16.8
Side chain	18.8
Solvent	7.02

All six molecules of the asymmetric unit were located by molecular replacement using chloroperoxidase 1a8s as a search model. After initial refinements including rigid-body refinement, conjugate-gradient minimization, torsion refinement and restrained individual *B*-factor refinement, the $3F_o - 2F_c$ electron density was well defined and allowed modeling of residues 1–271 in all six monomers of the asymmetric unit. Subsequent refinement of the model using *REFMAC* provided a model with excellent statistics (Table 1). The final model includes residues 1–271 in all monomers and solvent molecules including 1362 water molecules and 20 glycerol molecules. The electron-density map did not show the C-terminal His_6 tag included to simplify purification.

3.2. Structural description

3.2.1. Monomer. The PFE monomer is a roughly spherical globular protein with a diameter of ∼45 Å and a characteristic α/β-hydrolase fold (Ollis *et al.*, 1992; Fig. 2). Eight β-strands

with connectivity in Richardson notation (Richardson, 1981) of +1, +2, −1x, +2x, +1x, +1x, +1x form the β-sheet core of the protein. There are a total of ten α-helices that surround this sheet. Helices α1–α3 and α8–α10 correspond to helices *A*–*C* and *D*–*F*, respectively, of the canonical α/β-hydrolase fold. The large loop between strands β6 and β7 spans residues 120–219 and comprises five helices. Residues 138–208 in the β6–β7 loop form a hairpin with antiparallel packing of helix α4 with α7 and helix α5 with α6. Short loops connecting helices α4–α5 and helices α6–α7 allow a bend in the hairpin, resulting in a V-shape with one antiparallel helix pair in each arm of the V. The fifth helix in the loop, α8, corresponds to helix *D* of the canonical α/β-hydrolase fold (Ollis *et al.*, 1992). This V-shaped crossover between strands β6 and β7 (referred to throughout this paper as the β6–β7 loop) is topologically equivalent to the lid of *Pseudomonas* lipases (Schrag *et al.*, 1997). In lipases, the lid controls interfacial activation, but there is no evidence to suggest catalysis by PFE involves interfacial activation.

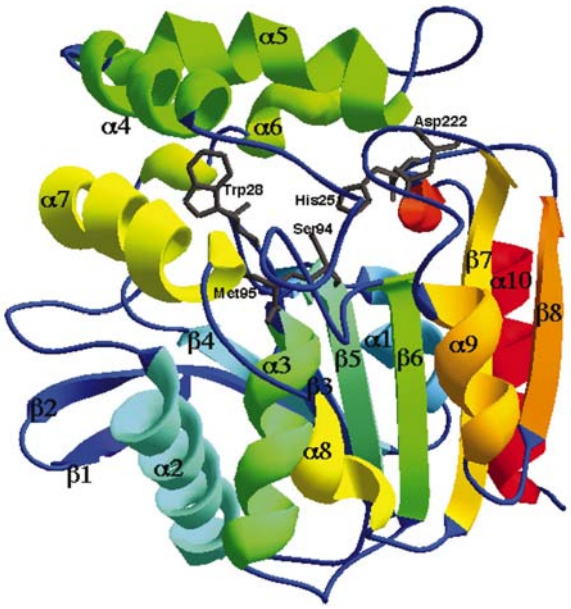

Figure 2
Ribbon diagram of the PFE monomer showing the active site colored in secondary-structure succession (progression through the visible spectrum from blue to red starting at the N-terminus). PFE is a typical α/β-hydrolase with catalytic triad Ser94, His251 and Asp222 and oxyanion-hole residues Trp28 and Met95 (stick representations) nearly totally obscured by the V-shaped β6–β7 loop (α4–α7 at the left and top of this picture). The eight β-strands form a sheet that provides the core of the protein and are labeled according to sequence succession. The C-terminal His_6 tag was not seen in the electron-density map. Note: Figs. 2, 3, 5 and 6 were produced with *Swiss PDB Viewer* (Guex & Peitsch, 1997).

3.2.2. Active site and surrounding area. Ser94, Asp222 and His251 form the catalytic triad of PFE (Fig. 3). The catalytic serine is located in a canonical nucleophile elbow in the conserved Gly-X_1-Ser-X_2-Gly sequence of esterases and lipases. In PFE, X_1 = Phe93 and X_2 = Met95. His251 and Asp222 are in positions consistent with a hydrolytic mechanism. The amide N—H of Trp28 (4.7 Å from Ser N^{α} to O^{γ}) and Met95 (3.0 Å from Ser N^{α} to O^{γ}) form the oxyanion hole. The active site is partly concealed by the β6–β7 loop, limiting direct access to small substrates in the absence of large conformational changes in the enzyme. The interior active-site surface encloses a small volume (<10 Å diameter), which shows two distinct binding pockets, one that could accommodate the acyl portion of an ester and one for the alcohol moiety (Figs. 3 and 4). The side chains of hydrophobic residues including Trp28, Val121 and Phe198 mainly form the acyl-binding pocket. Phe93 and Phe162 line the alcohol-binding pocket, which is also open to the solvent. A total of 694 $Å^2$ of water-accessible surface lies within a 10 Å radius of Ser94 (Connolly, 1983). Hydrophobic C atoms make up 78% of this area, while hydrophilic N, O and S atoms form the remaining 22%.

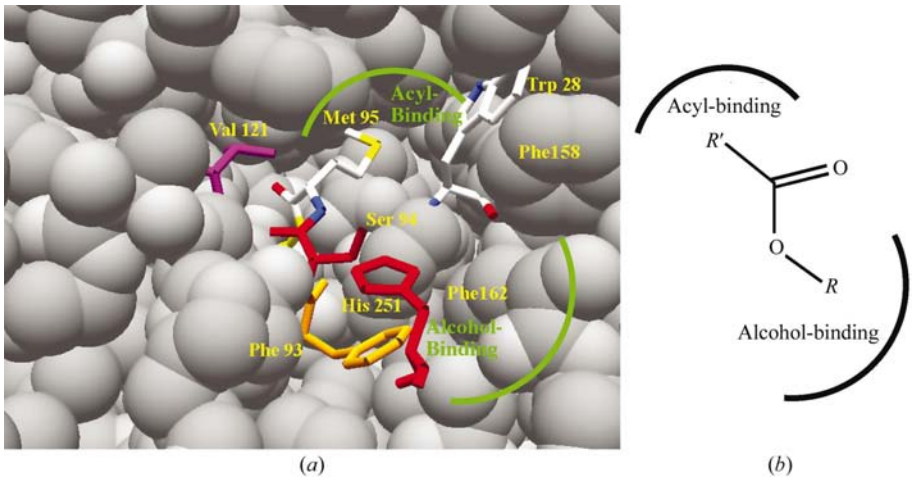

Figure 3
PFE active site for ester hydrolysis (*a*), with a schematic representation of the binding of an ester (*b*). The β6–β7 loop made of residues 138–208 normally limiting access to the triad is cut away for clarity, but otherwise completely covers this view. The orientation of the catalytic triad Ser94 (red), His251 (red) and Asp222 (not shown) are consistent with a hydrolytic mechanism. The amide N—H of Met95 and Trp28 (CPK colors) provide an oxyanion hole. Val121 at the left (violet) along with Trp28 (gray, space-filling) and Phe198 (not shown; lies in the β6–β7 loop) at the right limit the possible size of the R' group of the ester substrate. Aryl groups including Phe93 (orange) and Phe162 (gray, space-filling) create the alcohol-binding pocket surface (shown at right, bottom). All other residues are shown in gray space-filling representation.

3.2.3. Oligomers. Six PFE monomers, arranged as two trimers, form the asymmetric unit (Fig. 5). The r.m.s. deviation of the 271 C^{α} atoms between the six polypeptide chains in the asymmetric unit ranges from 0.11 to 0.27 Å. The buried surface area between monomers within a trimer is ~1500 $Å^2$, whereas the buried surface area between the two trimers is only ~800 $Å^2$. Crystal contacts involve several residues, most notably Pro129, Asp130, Tyr131 and Gln132, which are in the β6–β7 loop that occludes the active site. These crystal contacts may

influence the level to which the $\beta6$–$\beta7$ loop occludes the active site.

3.2.4. Comparisons with structural neighbors. A comparison of the C^{α} positions for chain *A* of PFE with known protein structures using *DALI* (Holm & Sander, 1993) revealed that the most similar proteins were not esterases, but non-heme bacterial haloperoxidases. The closest relative, with an r.m.s. deviation for 271 C^{α} atoms of 0.68 Å, is chloroperoxidase 1a8s from *P. fluorescens*. The next four closest relatives were bromoperoxidase 1a8q from *Streptomyces aureofaciens* (Hofmann *et al.*, 1998), with an r.m.s. deviation of 0.78 Å, and all three chains of chloroperoxidase 1a88 (Hofmann *et al.*, 1998) from *S. aureofaciens*, with an average r.m.s. deviation from the three of 0.86 Å. 1a8s also has a loop structure that limits access to the active site, but its loop does not conceal the active site to quite the extent as that of PFE (Fig. 4).

The active sites of 1a8s and PFE show similar amounts of hydrophobicity. Chloroperoxidase 1a8s has ~802 Å^2 of exposed surface within a 10 Å radius of Ser94, 69% of which is made of C atoms, compared with the ~694 Å^2 (78% C) surface of PFE. Non-conservative substitutions within 10 Å of Ser94 include (1a8s to PFE) Pro29 to Leu29, Ser34 to Met34, Met69 to Tyr69, Tyr72 to Phe72, Phe91 to Val91, Thr 95 to Met95, Met125 to Phe125 and Ser201 to Ala199. The Thr95 to Met95 is the substitution closest to the active sites (Fig. 6), but other haloperoxidases also have methionine in position 95 (*e.g.* 1a8q, Haag *et al.*, 1991). Thus, it is unlikely that the Thr/Met95 difference alone could account for the different catalytic activity. The shift in activity likely involves multiple substitutions, but additional experiments are needed to identify them.

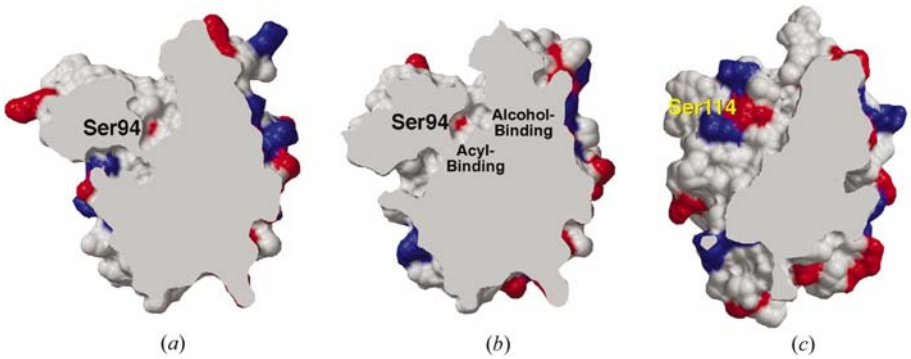

Figure 4
Surface plots of (*a*) chloroperoxidase 1a8s, (*b*) PFE and (*c*) carboxylesterase 1auo in similar orientations, showing differences in active-site accessibility. Basic residues are colored blue, acidic residues red and hydrophobic residues gray. The catalytic serine residue is a red patch immediately to the right of its label. The active site of 1a8s has a similar environment to that of PFE, but has a wider channel to the active site (at the top of this orientation). In both 1a8s and PFE, the loop that occludes the active site is seen at the top left (closing the channel that accesses the active site slightly more in PFE). Both PFE and 1a8s have a back-access channel located at the left of these orientations, with that of 1a8s nearly connecting with the main channel. 1auo lacks the loop structure, leaving the active site far more accessible. In PFE, the alcohol-binding pocket lies immediately to the left of its label and the acyl-binding pocket is directly above its label. The structures were superposed using *Swiss PDB Viewer* (Guex & Peitsch, 1997). Surfaces were calculated using *MSMS* (Sanner & Olson, 1996). The figures were produced using *POVSCRIPT* (Fenn *et al.*, 2003) and *RASTER3D* (Merritt & Murphy, 1994).

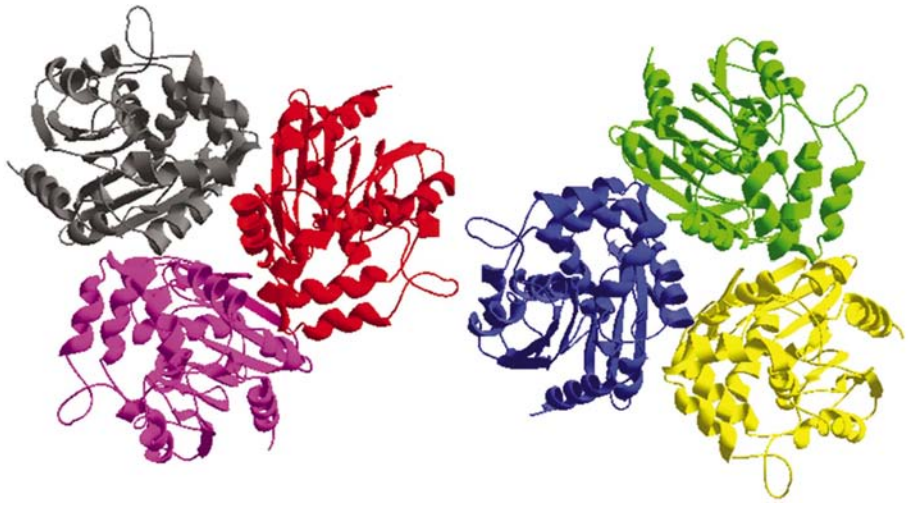

Figure 5
PFE crystal asymmetric unit showing the six chains. The unit cell was $P3_2$ with 72% solvent content. There are approximately twice as many interchain surface contacts between two monomers in a triad than between triads. The C-terminal region of all chains point away from one another; therefore, the His_6 tag does not cause this oligomeric arrangement.

In contrast, esterases show less structural similarity to PFE than the haloperoxidases, despite having similar catalytic activities. Carboxylesterase 1auo from *P. fluorescens* (Kim *et al.*, 1997), an enzyme discovered concurrently with PFE by Choi *et al.* (1990), shows the highest structural similarity of the esterases, with an r.m.s. deviation of 5.0 Å for 218 C^{α} atoms. The accessibility of the active site is the most obvious difference between these two esterases. The PFE active site is near the center of the roughly spherical enzyme and is obscured by the $\beta6$–$\beta7$ loop, whereas that of 1auo (Ser114, His199 and Asp168) is open to the solvent. 1auo has ~1190 Å^2 of water-accessible surface within a 10 Å radius of Ser114 and C atoms make up 56% of this surface. In contrast, PFE has a smaller water-accessible surface ~694 Å^2, which is more hydrophobic (78% C) (Fig. 4). The side chain of Gln115 forms one side of the acyl-binding pocket in 1auo. PFE has Trp28 in an analogous position, which restricts the acyl-binding pocket to smaller acyl groups. The alcohol-binding region in 1auo contains acidic residues and is open to the solvent. In contrast, PFE has mainly aromatic residues in the alcohol-binding region and is more

restricted, consistent with its known preference for aryl alcohol esters (Figs. 3 and 4). However, there is no obvious reason for the preference of PFE for activated esters.

4. Discussion

The structure of aryl esterase from *P. fluorescens*, solved to a resolution of 1.8 Å, reveals an α/β-hydrolase fold with characteristics typical of this structure family. PFE exhibits highest sequence identity and structural similarity toward several non-heme bacterial haloperoxidases. Its closest relative is chloroperoxidase 1a8s from *P. fluorescens*, which displays an r.m.s. deviation of 0.68 Å. The next four nearest structural neighbors are also haloperoxidases, with r.m.s. deviations in C^{α} of below 0.86 Å. PFE crystallized as a dimer of trimers. The crystal structure of chloroperoxidase 1a88 showed a similar single trimer, but most other haloperoxidases crystallized as single dimers. After the haloperoxidases, PFE shows next highest sequence identity to a group of esterases. The closest of these is carboxylesterase 1auo, also from *P. fluorescens*.

Pelletier & Altenbuchner (1995) found that in addition to esterase activity, PFE also has low haloperoxidase activity. Conversely, at least one of the non-heme haloperoxidases shows low esterase activity. This overlapping catalytic activity is not surprising given the mechanistic and structural similarities of esterases and haloperoxidases. A lactonase from *Actinobacter* also has significant bromoperoxidase activity (Kataoka *et al.*, 2000). The bromoperoxidase activity (199 U mg^{-1} with acetate and monochlorodimedon at pH 4.5) is only 24-fold lower than the lactonase activity (4760 U mg^{-1} with 3,4-dihydrocoumarin at pH 7) when both are measured at their optimal pH. Lipases also show haloperoxidase activity and Kirk & Conrad (1999) postulated that all esterases might show some haloperoxidase activity, bringing it into doubt whether non-heme haloperoxidases form a separate class of enzymes. On the other hand, soil bacteria secrete similar non-heme haloperoxidases in response to oxidative stress, suggesting that the haloperoxidase activity has a biological role (Barloy-Hubler *et al.*, 2004).

In spite of this overlap, esterase and lipase are more efficient at ester hydrolysis, while haloperoxidases are more efficient at generating peroxycarboxylic acids. PFE is particularly interesting as a possible evolutionary link because it is functionally more similar to the esterases but structurally more similar to the haloperoxidases. The structural basis for the higher esterase activity is not obvious from a comparison of 1a8s (a representative bacterial haloperoxidase) and PFE. Both have similar active-site pockets with similar amounts of hydrophobicity and similar restricted channels that lead to the active sites. Two differences are the higher accessibility of the 1a8s active site relative to that of PFE and a slightly more polar acyl-binding region in 1a8s, but it is not clear how these differences might influence catalytic activity. In the future, structures of bound transition-state analogues and site-directed mutagenesis of PFE to improve its haloperoxidase activity might reveal the origins of these differences.

The active site of PFE is smaller and less accessible than that of the most similar esterase by sequence and by structure, carboxylesterase 1auo from *P. fluorescens*. Bulky hydrophobic residues including Trp28 and Phe198 restrict the PFE acyl-binding pocket, whereas that of 1auo is open to solvent. This smaller acyl-binding pocket is consistent with the preference of PFE for esters with small acyl groups. The alcohol-binding pocket in PFE is lined with hydrophobic residues (including Phe93 and Phe162) compared with that of 1auo, which is open to the solvent. This lining of the alcohol-binding pocket with aromatic side chains is consistent with the preference of PFE for esters of aryl alcohols. The PFE active site is nearly occluded by the V-shaped $\alpha4$–$\alpha7$ part of the $\beta6$–$\beta7$ loop, consisting of residues 138–208. This active-site-blocking 70-residue section is missing in 1auo, which is 55 residues shorter than PFE. The 1auo active site is solvent-exposed and is accessible to substrates without conformational changes in the protein (Fig. 4).

PFE also accepts activated esters with large acyl groups, such as (*R*)-3-phenylbutyric acid resorufin ester (Henke & Bornscheuer, 1999). Accommodating these esters is surprising and is likely to require changes in the conformation. Two distant mutations increased the catalytic activity of PFE towards substrates with large acyl groups. A Leu180Gln mutation increased the activity and enantioselectivity of PFE towards (*R*)-3-phenylbutyric acid resorufin ester (Henke & Bornscheuer, 1999). The structure confirms that Leu180 is ~17 Å from the active site. It is on the enzyme surface close to the opening of the channel to the active site (Fig. 4) and in the turn between helices $\alpha6$ and $\alpha7$ in the $\beta6$–$\beta7$ loop. A double PFE mutant (Leu180Gln/Ala208Asp) increases the activity of PFE towards a sterically hindered 3-hydroxy ester (Bornscheuer *et al.*, 1999). Ala208 is at the opening of a back-access channel (Fig. 4) on helix $\alpha8$, which is between $\alpha7$ and $\beta7$ in a four-residue-long random-coil region of the $\beta6$–$\beta7$ loop. Both of these examples involve replacement of a hydrophobic amino acid by a hydrophilic amino acid (Leu180Gln and

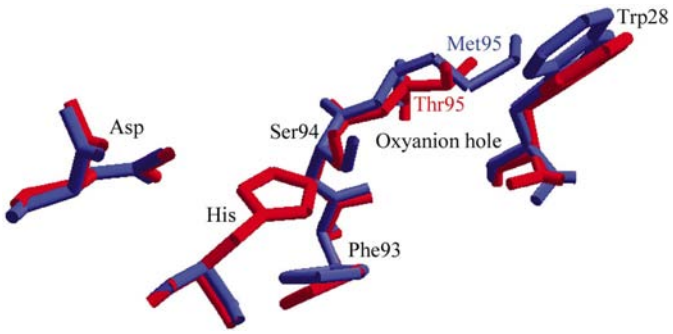

Figure 6
Active-site overlap of PFE and 1a8s highlighting the Thr95 (1a8s) to Met95 (PFE) change in the oxyanion hole. PFE is shown in blue, 1a8s in red. The catalytic triads of each (Ser94, His251, Asp 222 in PFE; Ser94, His253, Asp224 in 1a8s) are shown. The residues that make up the oxyanion hole are Trp28 in both PFE and 1a8s, with Met95 in PFE compared with Thr95 in 1a8s. The hydroxyl group of Thr95 of 1a8s points into the oxyanion hole and could make a hydrogen bond to an oxyanion (Hofmann *et al.*, 1998).

Ala208Asp). These changes may promote conformational changes that shift the $\beta6$–$\beta7$ loop and make the active site more accessible.

The structural basis for the enantioselectivity improvements towards methyl-(±)-3-bromo-2-methylpropionate (MBMP) caused by the Thr229Ile mutation (Horsman *et al.*, 2003) remain a mystery. The structure shows that Thr229 is 13 Å from the active site and does not contact the active site, binding pockets or access channels. The mutation may cause structural changes that propagate into the substrate-binding region. Site-directed mutagenesis of residues 28 (Trp) and 121 (Val) increased the enantioselectivity toward MBMP fivefold (Park *et al.*, 2004). The structure confirms that these residues interact directly with the acyl group.

5. Conclusion

The structure of the aryl esterase from *P. fluorescens* has been solved to a resolution of 1.8 Å by X-ray diffraction. Although this enzyme is an esterase, it also shows haloperoxidase activity. Its structure is most similar to a family of non-heme bacterial haloperoxidases, with highest sequence identity and structural similarity to chloroperoxidase 1a8s from *P. fluorescens*. The catalytic sites of PFE and the haloperoxidases are very similar, with PFE having a more occluded active site and a slightly less polar acyl-binding region. The catalytic sites of PFE and carboxylesterase show differences consistent with their different substrate specificity. PFE favors esters with small acyl groups and shows a restricted acyl-binding site. The structure of PFE also identifies residues where mutations may increase enantioselectivity of PFE for applications in biocatalysis.

We thank the Natural Sciences and Engineering Research Council (Canada) for funding, and Mirek Cygler for the use of the equipment and expertise at the Biotechnology Research Institute.

References

Barloy-Hubler, F., Cheron, A., Hellegouarch, A. & Galibert, F. (2004). *Microbiology*, **150**, 657–664.
Björkling, F., Frykman, H., Godtfredsen, S. E. & Kirk, O. (1992). *Tetrahedron*, **48**, 4587–4592.
Bornscheuer, U. T., Altenbuchner, J. & Meyer, H. H. (1999). *Bioorg. Med. Chem.* **7**, 2169–2173.
Brünger, A. T., Adams, P. D., Clore, G. M., DeLano, W. L., Gros, P., Grosse-Kunstleve, R. W., Jiang, J.-S., Kuszewski, J., Nilges, M., Pannu, N. S., Read, R. J., Rice, L. M., Simonson, T. & Warren, G. L. (1998). *Acta Cryst.* D**54**, 905–921.
Choi, K. D., Jeohn, G. H., Rhee, J. S. & Yoo, O. K. (1990). *Agric. Biol. Chem.* **54**, 2039–2045.
Connolly, M. L. (1983). *J. Appl. Cryst.* **16**, 548–558.
Fenn, T. D., Ringe, D. & Petsko, G. A. (2003). *J. Appl. Cryst.* **36**, 944–947.
Guex, N. & Peitsch, M. C. (1997). *Electrophoresis*, **18**, 2714–2723.
Haag, T., Lingens, F. & van Pée, K.-H. (1991). *Angew. Chem. Int. Ed. Engl.* **30**, 1487–1488.
Henke, E. & Bornscheuer, U. T. (1999). *Biol. Chem.* **380**, 1029–1033.
Hofmann, B., Tölzer, S., Pelletier, I., Altenbuchner, J., van Pée, K.-H. & Hecht, H.-J. (1998). *J. Mol. Biol.* **279**, 889–900.
Holm, L. & Sander, C. J. (1993). *J. Mol. Biol.* **233**, 123–128.
Horsman, G. P., Liu, A. M. F., Henke, E., Bornscheuer, U. T. & Kazlauskas, R. J. (2003). *Chemistry*, **9**, 1933–1939.
Kataoka, M., Honda, K. & Shimizu, S. (2000). *Eur. J. Biochem.* **267**, 3–10.
Kim, K. K., Song, H. K., Shin, D. H., Hwang, K. Y., Choe, S., Yoo, O. J. & Suh, S. W. (1997). *Structure*, **5**, 1571–1583.
Kirk, O. & Conrad, L. S. (1999). *Angew. Chem. Int. Ed.* **38**, 977–979.
Krebsfänger, N., Schierholz, K. & Bornscheuer, U. T. (1998). *J. Biotechnol.* **60**, 105–111.
Laatsch, H., Pudleiner, H., Pelizaeus, B. & van Pée, K. H. (1994). *Liebigs Ann. Chem.*, pp. 65–71.
Liu, A. M. F., Somers, N. A., Kazlauskas, R. J., Brush, T. S., Zocher, F., Enzelberger, M. M., Bornscheuer, U. T., Horsman, G. P., Mezzetti, A., Schmidt-Dannert, C. & Schmid, R. D. (2001). *Tetrahedron Asymm.* **12**, 545–556.
Merritt, E. A. & Murphy, M. E. P. (1994). *Acta Cryst.* D**50**, 869–873.
Murshudov, G. N., Vagin, A. A. & Dodson, E. J. (1997). *Acta Cryst.* D**53**, 240–255.
Ollis, D. J., Cheah, E., Cygler, M., Dijkstra, B., Frolow, F., Franken, S. M., Harel, M., Remington, S. J., Silman, I., Schrag, J., Sussman, J. L., Verschueren, K. H. G. & Goldman, A. (1992). *Protein Eng.* **5**, 197–211.
Park, S., Morley, K. M., Horsman, G. P., Holmquist, M., Hult, K. & Kazlauskas, R. J. (2004). In preparation.
Pelletier, I. & Altenbuchner, J. (1995). *Microbiology*, **141**, 459–468.
Pflugrath, J. W. (1999). *Acta Cryst.* D**55**, 1718–1725.
Picard, M., Gross, J., Lübbert, E., Tölzer, S., Krauss, S., van Pée, K.-H. & Berkessel, A. (1997). *Angew. Chem. Int. Ed. Engl.* **36**, 1196–1199.
Richardson, J. S. (1981). *Adv. Protein Chem.* **34**, 167–339.
Sanner, M. & Olson, A. J. (1996). *Biopolymers*, **38**, 305–320.
Schrag, J. D., Li, Y., Cygler, M., Lang, D., Burgdorf, H., Hecht, H.-J., Schmid, R., Schomburg, D., Rydel, T. J., Oliver, J. D., Strickland, L. C., Dunaway, C. M., Larson, S. B., Day, J. & McPherson, A. (1997). *Structure*, **5**, 187–202.
Vagin, A. & Teplyakov, A. (1997). *J. Appl. Cryst.* **30**, 1022–1025.